Local distortion in $LaCoO_3$ and $PrCoO_3$: extended x-ray absorption fine structure, x-ray diffraction and x-ray absorption near edge structure studies

2006 J. Phys.: Condens. Matter 18 10617

(http://iopscience.iop.org/0953-8984/18/47/008)

INSTITUTE OF PHYSICS PUBLISHING JOURNAL OF PHYSICS: CONDENSED MATTER

J. Phys.: Condens. Matter **18** (2006) 10617–10630 doi:10.1088/0953-8984/18/47/008

Local distortion in $LaCoO_3$ and $PrCoO_3$: extended x-ray absorption fine structure, x-ray diffraction and x-ray absorption near edge structure studies

S K Pandey[1], S Khalid[2], N P Lalla[1] and A V Pimpale[1]

[1] UGC-DAE Consortium for Scientific Research, University Campus, Khandwa Road, Indore 452 017, India
[2] National Synchrotron Light Source, Brookhaven National Laboratory, Upton, NY 11973, USA

E-mail: sk_iuc@rediffmail.com and avp@csr.ernet.in

Received 14 September 2006, in final form 18 October 2006
Published 13 November 2006
Online at stacks.iop.org/JPhysCM/18/10617

Abstract

Room temperature Co K edge extended x-ray absorption fine structure (EXAFS), x-ray absorption near edge structure (XANES), including the pre-edge structure, and x-ray diffraction (XRD) studies are carried out on $LaCoO_3$ and $PrCoO_3$. The Co–O, Co–La/Pr and Co–Co bond lengths are obtained from EXAFS analysis and compared with those obtained from XRD study. The EXAFS analysis of the data indicates that the CoO_6 octahedron is distorted in both $LaCoO_3$ and $PrCoO_3$. There are two Co–O bonds with bond length 1.863 (1.886) Å and four Co–O bonds with bond length 1.928 (1.942) Å for $LaCoO_3$ ($PrCoO_3$). Such distortion is expected in orthorhombic $PrCoO_3$ but not in rhombohedral $LaCoO_3$. This distortion in the CoO_6 octahedron is attributed to Jahn–Teller active Co^{3+} ions in an intermediate spin state in these compounds. Higher shell studies reveal that Debye–Waller (DW) factors of Co–Pr and Co–Co bonds in $PrCoO_3$ are greater in comparison with those of Co–La and Co–Co bonds in $LaCoO_3$, indicating that these bonds are structurally more disordered in $PrCoO_3$. The comparison of Co–Co bond lengths and corresponding DW factors indicates that the structural disorder plays an important role in deciding the insulating properties of these compounds. XANES studies have shown changes in the intensities and positions of different near edge features. The comparison of experimental spectra with the calculated ones—using the Co 4p density of states obtained from local density approximation calculations and matrix elements calculated using an atomic like core state as the initial state and a confluent hypergeometric function as the final state—indicates that for orthorhombic structure, the intensities of different features are lower as compared to those for the cubic structure. The pre-edge peaks attributed to Co 1s $\rightarrow$ $e_g^{\uparrow}$ and $e_g^{\downarrow}$ transitions show the effects of hybridization of the e_g orbitals with

O 2p orbitals, and their relative intensities in $PrCoO_3$ and $LaCoO_3$, can be explained by using the average Co–O bond length obtained from the EXAFS.

1. Introduction

Cobaltates with general formula $ACoO_3$ (A—rare earth element) form an interesting class of compounds in the perovskite family. They show temperature induced insulator to metal and non-magnetic to paramagnetic transitions [1–3]. The transport and magnetic properties of these compounds are dependent upon the spin state of the Co^{3+} ion, which is decided by the competition between the Hund's coupling energy and the crystal-field splitting energy [4]. These energies are comparable within a few meV and so thermal excitations can readily affect the occupancies of different e_g orbitals, thereby affecting the spin state of the Co^{3+} ion. As temperature increases these compounds show two main magnetic transitions: one at low temperatures around 100 K for $LaCoO_3$ and 200 K for $PrCoO_3$; and the other at high temperatures around 500 K for $LaCoO_3$ and 550 K for $PrCoO_3$. Earlier the high temperature transition was generally attributed to a high spin (HS) $t_{2g}^4e_g^2$ state and the low temperature transition to an admixture of HS and low spin (LS) $t_{2g}^6e_g^0$ states [5]. However, later on Potze *et al* introduced the concept of intermediate spin (IS) $t_{2g}^5e_g^1$ state in these compounds [6] and attributed the low temperature transition to LS to IS transition. Currently, it is generally believed that the spin state of the Co^{3+} ion changes from LS $\rightarrow$ IS $\rightarrow$ HS with increase in temperature.

The spin state of the Co^{3+} ion is closely related to the structural parameters of these compounds. It is well known that the ionic radius of an ion depends on its spin state. The lattice parameters of a perovskite depend on its tolerance factor, which is directly related to the ionic radii of various ions. Therefore, any change in spin state will directly affect the lattice parameters and thereby the unit cell volume, metal–oxygen bond lengths, etc [7]. At room temperature for both the compounds under study the Co^{3+} ion is in the IS state [8, 9]. In the IS state the e_g orbital possesses one electron, making Co^{3+} Jahn–Teller (JT) active, and it should influence the Co–O distances in the CoO_6 octahedron and distort it. Such distortion has been seen in manganites where the JT effect is important [10–12]. One expects similar structural distortion in the case of cobaltates with Co^{3+} in the IS state. X-ray and neutron powder diffraction studies of $LaCoO_3$ have shown the system to be rhombohedral at room temperature and hence the crystal symmetry demands the Co–O bond lengths be identical for all six bonds in the CoO_6 octahedron. To resolve the Co–O bond lengths through diffraction one needs to see the splitting of Bragg peaks which is limited by the experimental resolution. Pulsed neutron pair distribution function (PDF) studies have shown the existence of two Co–O bond lengths at 100 K [13]. For $PrCoO_3$, the x-ray structure is orthorhombic and one expects the Co–O bond lengths not to have to be the same. There are no neutron data on this compound to the best of our knowledge.

Extended x-ray absorption fine structure (EXAFS) observed about 50 eV above the main edge of the x-ray absorption (XA) spectrum contains information about the local structure around the absorbing/central atom. By analysing the EXAFS data one can get information about the bond lengths of the neighbouring atoms with respect to the central atom. The accuracy of the bond lengths determined from EXAFS data depends upon the photon energy range over which XA data are taken. The higher this range, the larger the photoelectron wavevector k range and the better our ability to distinguish between two very similar bond lengths. Thus high k range EXAFS data offer better opportunity to resolve bond lengths which

usual diffraction experiments cannot be used to do. Thus it is interesting to carry out EXAFS studies of cobaltates and compare the same with the x-ray diffraction studies.

The x-ray near edge structures (XANES) are sensitive to the electronic states of the absorbing atoms and the local structure through distribution of neighbouring atoms [14–17]. Recently we have studied the Co K and La L edges of $LaCoO_3$ and attributed different near edge features to the overlap of atomic orbitals of absorbing atoms with those of neighbouring atoms. The overlap of these orbitals is sensitive to the bond lengths. Therefore one expects changes in the XANES with change in the bond lengths. The changes in different near edge features in the doped compounds are generally attributed to change in local and electronic structures. The separation of these two contributions is rather difficult, as substitution of an atom for another atom changes the structure as well as the electronic states. However, the compounds under study seem to be good candidates for showing the effect of structure on the XANES as the electronic state of the Co ion is same at room temperature. Change in the rare earth site only changes the structural parameters due to change in the ionic radius without affecting much the electronic state of Co ions. Thus, simultaneous XANES and EXAFS studies of these compounds will throw some light on the influence of local structure on the XANES.

We report here room temperature Co K edge EXAFS, XANES and XRD studies of $LaCoO_3$ and $PrCoO_3$. The EXAFS results have shown distortion in the CoO_6 octahedron for both $LaCoO_3$ with rhombohedral structure and $PrCoO_3$ with orthorhombic structure. This distortion is attributed to the Jahn–Teller active Co^{3+} ion in the intermediate spin state in these compounds. The Debye–Waller factors of higher shells reveal that the $PrCoO_3$ has more structural disorder than $LaCoO_3$. XANES studies of these compounds show that the orthorhombic distortion decreases the intensity of the main edge and post-edge peaks. However, the intensity of pre-edge peaks for orthorhombic $PrCoO_3$ is seen to increase due to decreased overlap of Co e_g orbitals with O 2p orbitals as revealed by increase in the average Co–O bond length obtained from EXAFS.

2. Experiment and data analysis

The polycrystalline samples of $LaCoO_3$ and $PrCoO_3$ were prepared by the combustion method and characterized by x-ray diffraction (XRD) and resistivity techniques. The details of the sample preparation and characterization are given in our earlier publications [17–19]. Room temperature Co K edge XAS experiments were done at beamline X-18 B at the National Synchrotron Light Source, Brookhaven National Laboratory. The storage ring was operated at 2.8 GeV, 300 mA. The beamline used a Si(111) channel cut monochromator. The horizontal acceptance angle of the beam at the monochromator was 1 mrad. The vertical slit size used in this experiment was 1 mm, corresponding to an energy resolution of about 0.8 eV at the Co K edge. The average photon flux for this bandwidth was 10^{10} photons s^{-1}. The monochromator was detuned by 35% to reduce the higher harmonics. The incident (I_0) and the transmitted beam (I_t) were measured using sealed ion chambers, with a combination of gases for appropriate absorption. Standard Co foil was placed between the detectors I_t and I_{ref} for energy reference and to check the stability of the beamline and optical system. The samples sieved through a 400 mesh were spread uniformly on a cellophane tape and different layers of this tape were used to minimize the pinhole and brick effects. The pinhole corresponds to absence of the sample material and the brick corresponds to increased thickness of the absorber material in the path of the incident radiation. The value of $\mu x = \ln(I_0/I_t)$ would thus be different in the pinhole and the brick areas of the

sample: for the former it would be almost zero and for the latter it would be very large. Such inhomogeneity distorts the recorded spectra [20]. We have used two, three, and four layers of the sample adhered to cellophane tape and recorded the spectra. The Fourier analyses of the data for all three thicknesses showed exactly the same results indicating the uniformity of the sample thickness. The data given in this work correspond to four layers of the tape and the values of μx are in the range 0.87 to 1.4 for $LaCoO_3$ and 1.7 to 2.4 for $PrCoO_3$ around the main edge. The x-ray powder diffraction patterns were recorded with monochromatized Cu Kα radiation in the 2θ range of 10°–90° using a Rigaku powder x-ray diffractometer. The rotating anode x-ray generator was operated at 40 kV and 100 mA. The monochromator used was graphite (002) and the widths of the divergent slit, scattering slit and receiving slit were 0.5°, 0.5°, 0.15 mm, respectively. The data were collected with a step size of 0.02° with a scanning rate of 2° min^{-1}. To obtain the lattice parameters and atomic positions, XRD patterns were fitted using the Rietveld profile refinement technique [21]. The data were fitted by considering rhombohedral ($R\bar{3}c$) and orthorhombic ($Pnma$) structures for $LaCoO_3$ and $PrCoO_3$, respectively. The final refined lattice parameters match well with those reported in the literature. These refined lattice parameters and atomic positions were used as input parameters for the 'ATOM' program of the FEFF group to estimate the Co–O, Co–La/Pr and Co–Co bond lengths. Finally, the errors in the bond lengths were estimated by changing these input parameters by the amount of error in their values as yielded by the Rietveld program.

EXAFS fitting was carried out by using UWXAFS 3.0 software [22]. The threshold energy, E_0, for both the spectra was taken as the first inflection point in the absorption edge region. After the background subtraction, the absorption coefficient $\mu(E)$ was converted to $\mu(k)$, where $k = (2m(E - E_0)/\hbar^2)^{1/2}$ is the magnitude of the wavevector of the ejected photoelectron. The EXAFS oscillation $\chi(k)$ is defined as $(\mu - \mu_0)/\mu_0$, where μ_0 is the embedded atom absorption coefficient. The Fourier transformation (FT) to r space was in the k range 3–14 $Å^{-1}$, performed by Fourier transforming $k^2\chi(k)$ with the Hanning window. To find the local distortion in the CoO_6 octahedron, first shell fitting was done in the Fourier filtered k space in the range 0.65–1.90 Å for $LaCoO_3$ and 0.6–1.9 Å for $PrCoO_3$. We have used different model structures to get the information about the distortion in the CoO_6 octahedron. The average structure inferred from x-ray diffraction for $LaCoO_3$ is rhombohedral, implying that all six Co–O bonds of the CoO_6 octahedron are of equal length. First, we tried the *6 model* consisting of only one O shell with six equal Co–O bond lengths. As mentioned above, Louca *et al* [10] have reported the distorted CoO_6 octahedra at the local level with more than four short and less than two long bond lengths at 100 K in the IS spin state. Therefore, we also modelled local structure using the *4 +2 model* consisting of two shells with four equal short bond lengths and two equal long bond lengths. According to XRD results for $PrCoO_3$ the structure is orthorhombic and there are three Co–O bond lengths each corresponding to a pair of bonds: 1.901, 1.931, and 1.947 Å. As the last four bonds are nearly equal, in addition we used the *2 +4 model*, which consists of a two-shell fitting with two equal short bond lengths and four equal long bond lengths. The higher shell fitting was also carried out to get information about Co–La/Pr and Co–Co bond lengths. During this fitting the Co–O bond lengths were kept fixed at their values obtained from two-shell fitting over the CoO_6 octahedron. To get reliable information about these bond lengths we have not considered the distribution of bonds in each shell and only single scattering was considered, as such considerations would enhance the number of variable parameters and corresponding paths. Thus we have concentrated on getting the average bond lengths of each higher shell. For this purpose we have carried out the higher shell fitting by considering two shells for eight Co–La/Pr bonds and one shell for six Co–Co bonds in the Fourier filtered k space in the range 0.65–3.85 Å for $LaCoO_3$ and

0.6–3.9 Å for $PrCoO_3$. The overall many body reduction factor S_0^2 arises from the overlap contribution of the passive electrons. It is typically around 0.7 to 0.9 and it is not very sensitive to the chemical environment. For $La_{1-x}Sr_xMnO_3$, the value of $S_0^2 = 0.82$ was used in our earlier work [11] as it gave the best fit. We have adopted the same value for both $LaCoO_3$ and $PrCoO_3$, as replacing Mn by Co is not expected to change this value significantly. Our results also show that the chosen value of $S_0^2 = 0.82$ gave the best fit. The back-scattering amplitude and phase shifts were calculated using FEFF6.01 [23]. During the fitting the number of atoms in the different coordination shells (N) was kept fixed as per the choice of model structure and only bond lengths and corresponding Debye–Waller factors (σ^2) were varied to reduce the number of correlated parameters. Further, several different fits were performed in each case to verify the robustness of the parameters. Both simultaneous variation of different fitting parameters and independent variations were tried. A fit is considered to be good if the goodness of fit given by the R-factor is less than 0.02 [22]. Since for each compound fitting was tried using different structure models, the model that resulted in the least R-factor was considered to represent best the local structure for that particular compound. The bond lengths and the errors in their values are yielded directly by the fitting program when the bond lengths are varied for fitting purposes.

3. Computational details

Spin polarized local density approximation (LDA) band structure calculations for $LaCoO_3$ were carried out using LMTART 6.61 [24]. Rhombohedral $LaCoO_3$ is modelled for simplicity by a cubic perovskite structure with lattice parameters corresponding to double the Co–O bond length obtained from XRD. To see the effect of lattice distortion on the XANES we have also considered orthorhombically distorted perovskite structure with lattice parameters taken as double the Co–O bond length obtained from XRD for $PrCoO_3$. For calculating the charge density, the full-potential LMTO method working in the plane wave representation was used. The muffin-tin radii used in the calculations are 3.509, 2.001, and 1.637 au for La, Co, and O sites, respectively. The charge density and effective potential were expanded in spherical harmonics up to $l = 6$ inside the sphere and in a Fourier series in the interstitial region. The initial basis set included: 6s, 6p, 5d, and 4f valence and 5s, 5p semicore orbitals of La; 4s, 4p, and 3d valence and 3p semicore orbitals of Co; and 2s and 2p valence orbitals of O. The exchange–correlation functional of the density functional theory was taken after Vosko *et al* [25]. (6, 6, 6) divisions of the Brillouin zone along three directions for the tetrahedron integration were used to calculate the DOS. Self-consistency was achieved by demanding the convergence of the total energy to be smaller than 10^{-5} Ryd/cell.

Under the dipole approximation the K edge absorption process occurs due to transition of an electron from an s symmetric state to a p symmetric unoccupied state. Due to the participation of localized states in the transition the contribution of states of atoms other than the Co to the Co K edge absorption is negligible. Thus Co K edge absorption can be identified with the electronic transition from Co 1s to 4p states. To calculate the absorption spectra we need the matrix elements and DOS of Co 4p states. We have calculated the matrix element $\langle\psi_F|H_{int}|\psi_I\rangle$ by using $|\psi_I\rangle$ as the 1s hydrogenic wavefunction and $|\psi_F\rangle$ as the confluent hypergeometric function [26]. The matrix element thus obtained has been used to obtain the transition probability per second (w). To calculate the absorption spectrum, calculated w is convoluted with a Lorentzian having FWHM 2.1 eV to account for the lifetime of the Co 1s core hole generated during the absorption process [27] and a Gaussian having FWHM 2 eV to account for the instrumental and other broadening.

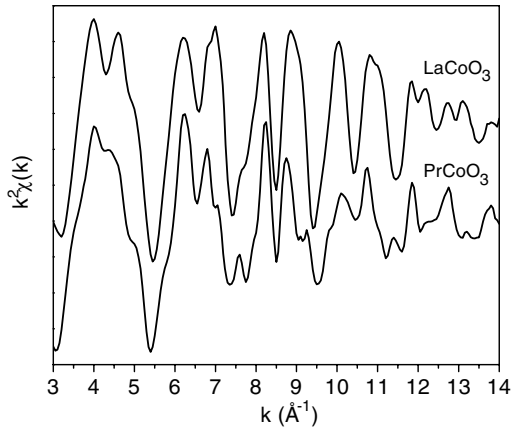

Figure 1. k^2 weighted EXAFS spectra $\chi(k)$ of $LaCoO_3$ (upper) and $PrCoO_3$ (lower).

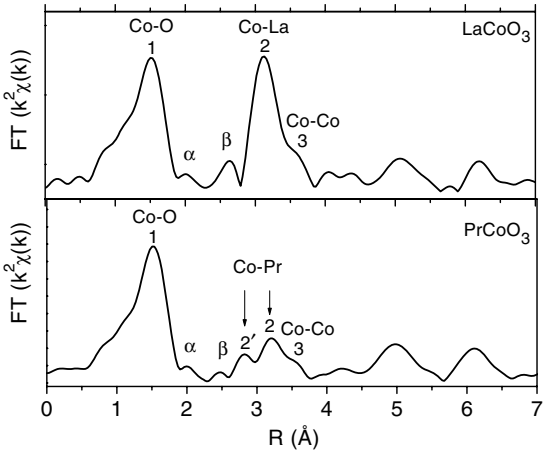

Figure 2. Fourier transforms of $k^2\chi(k)$ for $LaCoO_3$ (upper panel) and $PrCoO_3$ (lower panel).

4. Results and discussion

4.1. EXAFS

Figure 1 shows the k^2 weighted Co K edge EXAFS spectra $\chi(k)$ for $LaCoO_3$ and $PrCoO_3$. The k range used for analysis is from 3 to 14 $Å^{-1}$. Both the spectra are highly structured as expected from the powder crystal nature of the samples. As one goes from $LaCoO_3$ to $PrCoO_3$ there is appreciable change in the spectrum indicating changes in the local structure around Co sites. The FT of both the $k^2\chi(k)$ spectra are shown in figure 2. These spectra are uncorrected for the central and back-scattered phase shifts. We have fitted the spectra in the r range 0.6 to 3.9 Å; for $r < 0.6$ Å the data reveal structure due to the limited k range and for $r > 3.9$ Å one has to go to higher coordination shells. In this range for $LaCoO_3$ we observe three main peaks marked by 1, 2 and 3 ascribed to the first, second and third coordination shells of the central Co atom comprising the six O atoms of the CoO_6 octahedron, eight La atoms and six Co atoms, respectively as per expectations from perovskite structure. For $PrCoO_3$ we observe four main peaks denoted by 1, 2′, 2, and 3. Peaks 1 and 3 correspond to Co–O and Co–Co

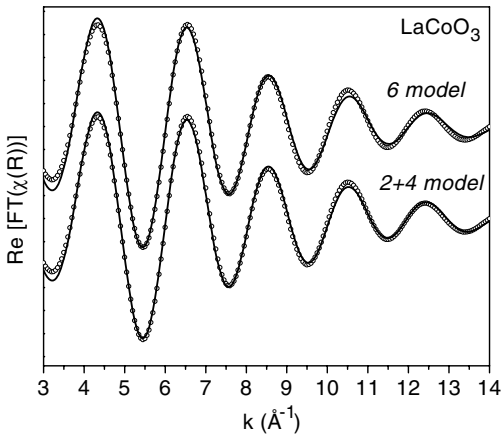

Figure 3. Fitted patterns of $LaCoO_3$ using the *6 model* having six equal Co–O bonds and the *2 +4 model* having two short and four long Co–O bonds.

shells. Peak 2 corresponding to the second coordination shell of central Co atom surrounded by eight La atoms in $LaCoO_3$ is well split into two peaks in the $PrCoO_3$ denoted by $2'$ and 2. The intensities of the peaks $2'$, 2 and 3 are significantly lower for $PrCoO_3$ indicating the increased local disorder for second and third shells in comparison to that for $LaCoO_3$. The XRD results revealed rhombohedral structure for $LaCoO_3$ and orthorhombic structure for $PrCoO_3$. In the rhombohedral structure out of eight Co–La bonds, two are at 3.273 Å and the remaining six are at 3.325 Å, whereas for orthorhombic structure the eight bonds are at 3.140, 3.250, 3.333, and 3.411 Å with two each at the same distance. Similarly, all six Co–Co bonds are exactly at equal distance (3.825 Å) in the rhombohedral structure, whereas in the orthorhombic they split into two groups with two bonds at 3.787 Å and the remaining four at 3.789 Å. Thus one expects more disorder in the $PrCoO_3$ due to its orthorhombic structure. The two peaks α and β observed between peaks 1 and 2 ($2'$ for $PrCoO_3$) are attributed to spectral leakage and double-scattering peaks corresponding to Co–O–O–Co.

The single- and double-shell fits over the CoO_6 octahedron for $LaCoO_3$ and $PrCoO_3$ are shown in figures 3 and 4, respectively. It is clear from the figures that the *6 model* which considers all six Co–O bonds at the same distance does not give a good fit at higher k values. On considering the *2 +4 model*—where two short bonds are at same distance and the remaining four bonds are long and at the same distance—the fit improves. We have also tried the *4 +2 model*, which considers four short bonds at equal distances and the remaining two long and at the same distance; however, this model does not improve the fit. Thus, the *2 +4 model* is a better representative of the experimental data. Parameters obtained from the fitting are given in table 1. It is clear from the table that the difference between the long and short bonds is 0.065 Å for $LaCoO_3$ whereas for $PrCoO_3$ it is 0.056 Å. This difference is well beyond the accuracy 0.008 Å of the bond length. Thus, $LaCoO_3$ is slightly more distorted at the local level. The distortion in the CoO_6 octahedron at the local level is interesting for $LaCoO_3$ as its structure is rhombohedral. In the rhombohedral structure one would expect all six Co–O bonds to be of equal length. Such a distribution in bond length of the CoO_6 octahedron at the local level may be direct evidence of the JT distortion expected in these compounds with Co^{3+} ions in the IS state. In this state one electron goes to the e_g level making the Co^{3+} ion JT active. Louca *et al* [10] and Maris *et al* [28] have also seen distortion in the CoO_6 octahedron in $LaCoO_3$. Louca *et al* have carried out temperature dependent PDF studies using pulsed neutrons on a powder

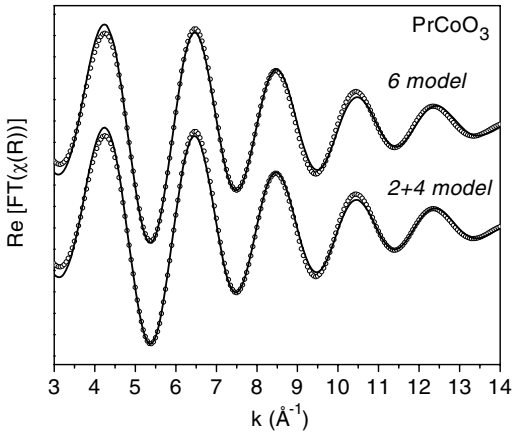

Figure 4. Fitted patterns of $PrCoO_3$ using the *6 model* having six equal Co–O bonds and the *2 +4 model* having two short and four long Co–O bonds.

Table 1. The Co–O bond lengths, Debye–Waller (DW) factors, and *R*-factors of $LaCoO_3$ and $PrCoO_3$ obtained from EXAFS analysis. The average Co–O bond lengths obtained from XRD are also given.

	$LaCoO_3$			$PrCoO_3$		
	Bond length (Å)	DW factor ($\times 10^{-3}$ Å^2)	*R*-factor	Bond length (Å)	DW factor ($\times 10^{-3}$ Å^2)	*R*-factor
6 model	6 × 1.914(1)	4.1(2)	0.0040	6 × 1.921(2)	3.5(4)	0.0056
2 +4 model	2 × 1.863(6)	4.5(8)		2 × 1.886(8)	3.0(1.2)	
	4 × 1.928(2)	2.3(4)	0.0025	4 × 1.942(4)	2.7(6)	0.0048
Average	6 × 1.906			6 × 1.923		
XRD	6 × 1.936(5)			6× 1.926(4)		

sample. They have seen two peaks at 1.915 and 2.16 Å corresponding to two bond lengths at 100 K. The area under these peaks gives information about the number of equal bonds and the sum of these areas is normalized to six; the number of short bonds is greater than four and the number of long bonds correspondingly is lower than two. They have seen a decrease in the area of the peak at 2.16 Å with increase in temperature and this peak merges almost into the background at 300 K. The experiment of Maris *et al* dealt with high resolution single-crystal XRD studies with synchrotron radiation. They noted monoclinic distortion with three different Co–O bond lengths. Unlike what Louca *et al* found, the distortion increased to a higher value as temperature increased to room temperature. Our room temperature EXAFS studies also reveal that there is a distortion in the CoO_6 octahedron and the nature of the distortion is different from that obtained from Louca *et al* [10] at 100 K. In our case there are two short bonds at 1.863 Å and four long bonds at 1.928 Å. It is interesting that these short and long bond lengths are closer to the short and middle bond lengths of Maris *et al* at 295 K. They have attributed this distortion to the cooperative JT effect.

The higher shell fittings were performed on $LaCoO_3$ and $PrCoO_3$ data to find the average Co–La/Pr and Co–Co bond lengths; the Co–O bond lengths were kept fixed to the values obtained from the first shell fitting. These fits are plotted in figures 5 and 6 for $LaCoO_3$

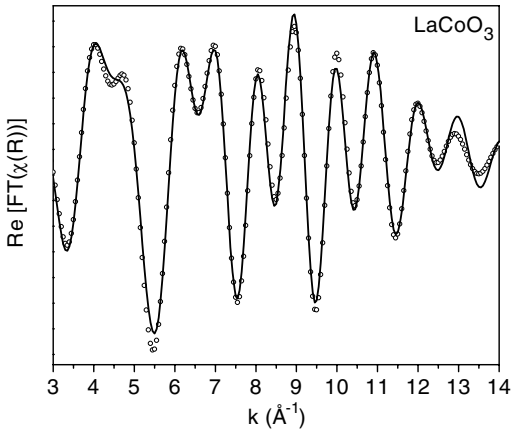

Figure 5. Higher shell fitted pattern of $LaCoO_3$ including Co–O, Co–La and Co–Co shells.

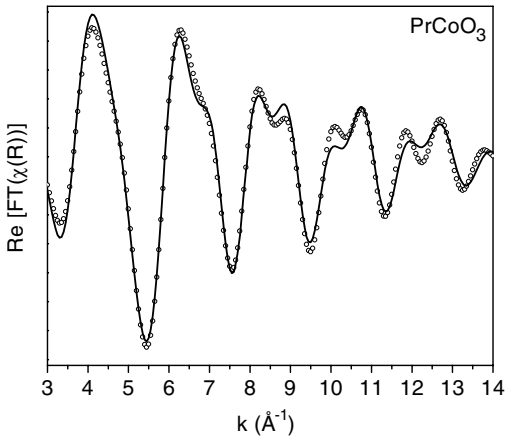

Figure 6. Higher shell fitted pattern of $PrCoO_3$ including Co–O, Co–Pr and Co–Co shells.

and $PrCoO_3$, respectively. It is clear from the figure that the fitted data deviate from the experimental ones at higher k, indicating that there is a distribution in these bond lengths as well at the local level. The deviation is greater for $PrCoO_3$, suggesting that the distribution in bond lengths is greater in this compound. Parameters obtained from fitting are given in tables 1 and 2. Bond lengths obtained from XRD are also given in these tables. It is seen that for $LaCoO_3$ there are six Co–O bonds at average length 1.906 Å, two Co–La bonds at 3.251 Å and the remaining six Co–La bonds at 3.334 Å and six Co–Co bonds at 3.894 Å. For $PrCoO_3$ there are six Co–O bonds at average length 1.923 Å, two Co–Pr bonds at 3.128 Å and the remaining six Co–Pr bonds at 3.308 Å and six Co–Co bonds at 3.818 Å. This indicates that the average Co–O bond length in $PrCoO_3$ is more than that in $LaCoO_3$ whereas the other bond lengths are small in comparison to those of $LaCoO_3$. Here it is important to note that the difference between two Co–Pr bonds is 0.18 Å which is more than the EXAFS resolution $\Delta R = \pi/[2(k_{max} - k_{min})] \approx 0.143$ Å, and we were able to see two experimentally well resolved peaks $2'$ and 2 corresponding the two and six Co–Pr bonds, respectively. The Debye–Waller (DW) factor for the Co–Pr bond is higher than the corresponding factor for the Co–La bond

Table 2. The Co–La/Pr and Co–Co bond lengths, Debye–Waller (DW) factors, and *R*-factors of $LaCoO_3$ and $PrCoO_3$ obtained from EXAFS analysis. The average Co–La/Pr and Co–Co bond lengths obtained from XRD are also given.

		EXAFS			XRD
Compound	Type of bond	Bond length (Å)	DW factor ($\times 10^{-3}$ Å^2)	*R*-factor	Bond length (Å)
$LaCoO_3$	Co–La	2 × 3.251(17)	5.0(1.5)		2 × 3.273(1)
		6 × 3.334(5)	4.6(5)	0.012	6 × 3.325(1)
	Co–Co	6 × 3.894(9)	6.5(7)		6 × 3.825(1)
$PrCoO_3$	Co–Pr	2 × 3.128(16)	7.0(2.6)		2× 3.140(8)
		6 × 3.308(7)	10.0(1.1)	0.015	6 × 3.331(3)
	Co–Co	6 × 3.818(8)	9.0(1.0)		6 × 3.788(1)

indicating higher disorder in $PrCoO_3$ as compared to $LaCoO_3$. As the thermal contributions to the disorder would be almost the same in the two cases, it may be inferred that the structural disorder is greater for Co–Pr bonds as compared to Co–La bonds. Similarly the DW factor corresponding to Co–Co bonds is higher for $PrCoO_3$ suggesting that this shell is also more disordered at the local level in $PrCoO_3$ in comparison to $LaCoO_3$. This result is quite interesting in the light of the insulating behaviour of these compounds as $PrCoO_3$ is more insulating than $LaCoO_3$ [29]. The insulating property is governed by the probability of electron hopping from one Co site to the next Co site, and the higher the bond length the lower the overlap of the electronic wavefunctions, and the smaller the hopping probability, leading to higher resistivity. The Co–Co bond length in $PrCoO_3$ is less; therefore one expects $PrCoO_3$ to be less insulating than $LaCoO_3$ contrary to the experimental situation [29]. Thus it seems that, besides the bond length, the higher structural disorder in $PrCoO_3$ plays an important role in the transport behaviour.

The comparison of the bond lengths obtained from EXAFS and XRD is quite interesting. It is seen from table 1 that the XRD Co–O bond length is higher in $LaCoO_3$ as compared to that in $PrCoO_3$, whereas the EXAFS Co–O bond length is higher in $PrCoO_3$. The XRD bond lengths obtained from powder data are constrained by the assumed model of the crystal structure—rhombohedral for $LaCoO_3$ and orthorhombic for $PrCoO_3$—whereas EXAFS analysis permitted the existence of distortion in the CoO_6 octahedron. The validity of the EXAFS result is reinforced by its application in the interpretation of the XANES in these compounds as discussed in the next section. The comparison of average Co–La/Pr and Co–Co bond lengths obtained from the EXAFS and XRD given in table 2 indicates that the local structure is different from the average crystal structure.

4.2. XANES

The experimental x-ray absorption spectra of $LaCoO_3$ and $PrCoO_3$ are shown in figure 7. The spectra have been normalized to unity at 100 eV above the edge. One can see nine features in the spectra denoted as A, B, C, D, E, F, G, H, and I. Two features A and B are pre-edge structures and were earlier attributed to Co 1s $\rightarrow$ $e_g^{\uparrow}$ and $e_g^{\downarrow}$ transitions [17]. Part of the Co K edge XANES in $LaCoO_3$ was also discussed in this work. However, the energy range in the present work is higher and the results are interpreted using DOS calculations under the LDA. The rest of the features correspond to the transition of an electron from the Co 1s $\rightarrow$ 4p orbital hybridized with different orbitals. The pre-edge peaks have been plotted in the inset on a zoomed scale. It is clear from the inset that the intensity of peak B slightly increases for

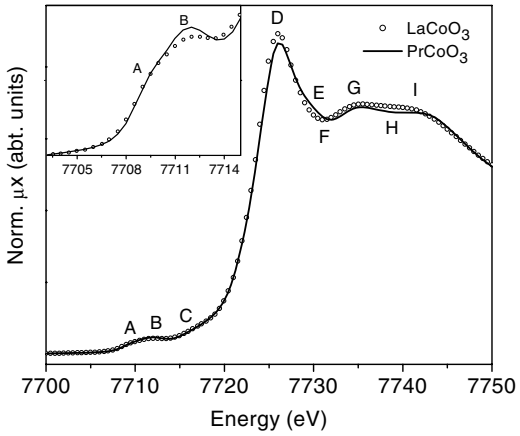

Figure 7. Normalized Co K edge XANES spectra of $LaCoO_3$ and $PrCoO_3$ indicated by open circles and a solid line, respectively. The inset shows zoomed two pre-edge structures denoted as A and B.

$PrCoO_3$. The intensities of peaks D and G decrease whereas the intensity of peak I remains almost the same. Moreover, hump E and dip H are more prominent for $PrCoO_3$. Slight shifts in the positions of features F, G, H, and I to the higher energy side are also seen.

The sensitivity of the XANES to local structure has been shown by many workers [14–16]. To see the effect of lattice distortion on different XANES features we have calculated the absorption spectra for cubic and orthorhombic distortion. These spectra are plotted in the upper panel of figure 8 along with the experimental data. Experimental spectra are rigidly shifted to match the positions of the main peaks with the calculated ones. It is clear from the figure that all the features except the two pre-edge features observed in the experimental spectra are also present in the calculated ones with slight deviations in the energy positions. The partial densities of states (PDOS) of La 6p, Co 4p, and O 2p are also plotted in the lower panel of figure 8. By looking at the PDOS one can see that in the energy region between structures C and D the La 6p DOS is dominating; thus this region can be attributed to transition to the Co 4p state strongly hybridized with the La 6p state. However, in the energy region between features D and E the contributions of the La 6p and O 2p DOS are almost the same. Therefore, this region is attributed to the Co 4p state hybridized with La 6p and O 2p states. Similarly, the region between structures E and F can be attributed to Co 4p hybridized with La 6p and O 2p states. In this region the contribution of La 6p is more in the hybridization in comparison to O 2p, as the La 6p DOS is about 3 times more than that of O 2p. Structure G is attributed to the hybridized La 6p, Co 4p, and O 2p states, whereas structure I is attributed to Co 4p state hybridized with the O 2p state.

It is evident from the upper panel of figure 8 that the spectra calculated by taking cubic and orthorhombic structures into account are representatives of the experimental spectra of $LaCoO_3$ and $PrCoO_3$, respectively. It may be noted that although the different features in the experimental spectrum match with the corresponding features in the calculated spectrum, there is a considerable difference in post-edge intensity. This may be due to the fact that the calculation of the matrix element was done by considering atomic states only, rather than the solid-state wavefunction involving hybridization of the Co 4p state with other states. Moreover, the absolute intensity of the absorption spectrum depends on effects like inelastic losses, extrinsic losses etc. It may be mentioned that such disagreement in experiment and calculation is quite well known in the literature and Rehr and Albers [30] have commented

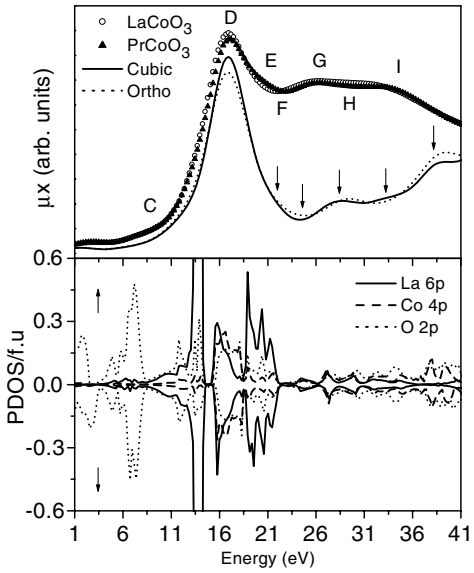

Figure 8. Normalized Co K edge XANES spectra of $LaCoO_3$ and $PrCoO_3$ indicated by open circles and triangles, respectively, and spectra calculated by taking cubic and orthorhombic structures, denoted by solid and dotted lines, respectively, are shown in the upper panel. The post-edge features in the calculated spectra corresponding to experimental ones are indicated by arrows. In the lower panel La 6p (solid lines), Co 4p (dashed lines), and O 2p (dotted lines), the density of states per formula unit for different spin polarizations is shown.

on it as one of the challenging problems in the field. The intensity of the main edge peak D decreases for the orthorhombic structure in conformity with the observed decrease in the intensity of peak D for $PrCoO_3$. One can see overall a small decrease in intensity in the region of peak G, whereas in the region of peak I the intensity increases. Moreover, orthorhombic distortion also shifts the positions of peaks G and I and dips F and H as observed experimentally for $PrCoO_3$. It is also clear from the calculated spectra that the features E and H are more prominent in the orthorhombic structure, as seen experimentally. Thus spectra calculated by considering cubic and orthorhombic structures follow the experimental data for $LaCoO_3$ and $PrCoO_3$, respectively. It is thus seen that the orthorhombic distortion decreases the intensity of the main peak D and affects the intensity as well as the position of the post-edge peaks. Our calculated spectra closely follow the changed behaviour of all the peaks except peak I when one goes from $LaCoO_3$ to $PrCoO_3$. In the case of peak I the intensity of this peak increases for orthorhombic structure, which is opposite to the observed behaviour. This may be due to limitations of our calculations.

Finally, we comment on the increased intensity of the pre-edge peaks for $PrCoO_3$. As mentioned earlier the two pre-edge structures are attributable to Co 1s $\rightarrow e_g^{\uparrow}$ and $e_g^{\downarrow}$ transitions. As seen from calculations, the e_g orbitals are strongly hybridized with O 2p orbitals and their atomic character is thereby affected. Thus the higher the admixture with O 2p, the lower the Co e_g atomic character and the lower the intensity of the pre-edge peaks. This admixture is directly proportional to the average Co–O bond length. Thus the observed higher intensities of the pre-edge peaks in $PrCoO_3$ as compared to $LaCoO_3$ are in conformity with the EXAFS Co–O distances in these compounds rather than the XRD Co–O bond lengths. This is also as per the known sensitivity of the XANES to the local order.

5. Summary and concluding remarks

Room temperature Co K edge EXAFS and XANES studies have been carried out on $LaCoO_3$ and $PrCoO_3$. The powder x-ray diffraction studies have shown the crystal structures of $LaCoO_3$ and $PrCoO_3$ to be rhombohedral and orthorhombic, respectively. In the rhombohedral structure all six Co–O bond lengths should be equal; however, EXAFS analysis of $LaCoO_3$ data has revealed two different bond lengths, making the CoO_6 octahedron distorted. The EXAFS studies of $PrCoO_3$ have also shown a similarly distorted CoO_6 octahedron. This distortion in the octahedron at room temperature is attributed to the effect of Co^{3+} ions in intermediate spin states, making it Jahn–Teller active. The higher shell fitting reveals that the Co–Co bond length in $LaCoO_3$ is greater in comparison to that in $PrCoO_3$; however, higher values of the Debye–Waller (DW) factor of this bond in $PrCoO_3$ indicate that this bond has more structural disorder in $PrCoO_3$ than in $LaCoO_3$. Such behaviour is also seen for Co–La/Pr bonds. This behaviour of the bond lengths and DW factors indicates that structural disorder is playing an important role in governing the increased resistivity of $PrCoO_3$ as compared to $LaCoO_3$. XANES studies of these compounds revealed the influence of crystal structure in deciding the intensities and energy positions of different features. The comparison of experimental and calculated spectra show that the intensity of the main edge and post-edge peaks decreases in orthorhombic structures, as observed for $PrCoO_3$. The pre-edge peaks observed for both compounds are attributed to Co 1s $\rightarrow$ $e_g^{\uparrow}$ and $e_g^{\downarrow}$ transitions. The intensity of pre-edge peaks is seen to be greater for $PrCoO_3$. This increase in intensity has been explained by using the average Co–O bond length obtained from the EXAFS rather than that from the XRD. According to the EXAFS the Co–O bond length is greater for $PrCoO_3$ making Co e_g orbitals less hybridized with O 2p orbitals. This decrease in overlap of these two orbitals enhances the atomic character of the e_g orbital resulting in increased intensity due to increase in the matrix element. This result indicates the sensitivity of pre-edge features to the local distribution of surrounding atoms.

Acknowledgments

We would like to acknowledge R Rawat for resistivity measurements. SKP thanks UGC-DAE CSR for financial support.

References

[1] Raccah P M and Goodenough J B 1967 *Phys. Rev.* **155** 932
[2] Yamaguchi S, Okimoto Y, Taniguchi H and Tokura Y 1996 *Phys. Rev.* B **53** R2926
[3] Plakhty V P, Brown P J, Grenier B, Shiryaev S V, Barilo S N, Gavrilov S V and Ressouche E 2006 *J. Phys.: Condens. Matter* **18** 3517
[4] Imada M, Fujimori A and Tokura Y 1998 *Rev. Mod. Phys.* **70** 1039
[5] Goodenough J B 1957 *J. Phys. Chem. Solids* **6** 287
[6] Potze R H, Sawatzky G A and Abbate M 1995 *Phys. Rev.* B **51** 11501
[7] Radaelli P G and Cheong S-W 2002 *Phys. Rev.* B **66** 094408
[8] Korotin M A, Ezhov S Yu, Solovyev I V, Anisimov V I, Khomskii D I and Sawatzky G A 1996 *Phys. Rev.* B **54** 5309
[9] Yan J-Q, Zhou J-S and Goodenough J B 2004 *Phys. Rev.* B **69** 134409
[10] Louca D, Egami T, Brosha E L, Roder H and Bishop A R 1997 *Phys. Rev.* B **56** R8475
[11] Bindu R, Pandey S K, Kumar A, Khalid S and Pimpale A V 2005 *J. Phys.: Condens. Matter* **17** 6393
[12] Shibata T, Bunker B A and Mitchell J F 2003 *Phys. Rev.* B **68** 024103
[13] Louca D, Sarrao J L, Thompson J D, Röder H and Kwei G H 1999 *Phys. Rev.* B **60** 10378
[14] Wu Z Y, Benfatto M, Pedio M, Cimino R, Mobilio S, Barman S R, Maiti K and Sarma D D 1997 *Phys. Rev.* B **56** 2228

[15] Ignatov A Yu, Ali N and Khalid S 2001 *Phys. Rev.* B **64** 014413
[16] Vedrinskii R V, Kraizman V L, Novakovich A A, Demekhin Ph V and Urazhdin S V 1998 *J. Phys.: Condens. Matter* **10** 9561
[17] Pandey S K, Kumar A, Khalid S and Pimpale A V 2006 *J. Phys.: Condens. Matter* **18** 7103
[18] Pandey S K, Bindu R, Bhatt P, Chaudhari S M and Pimpale A V 2005 *Physica* B **365** 45
[19] Pandey S K, Kumar A, Chaudhari S M and Pimpale A V 2006 *J. Phys.: Condens. Matter* **18** 1313
[20] Stern E A and Kim K 1981 *Phys. Rev.* B **23** 3781
[21] Young R A and Sakthivel A 1988 *J. Appl. Crystallogr.* **21** 416
[22] Stern E A, Newville M, Ravel B, Yacoby Y and Haskel D 1995 *Physica* B **208/209** 117
[23] Zabinsky S R, Rehr J J, Ankudinov A, Albers R C and Eller M J 1995 *Phys. Rev.* B **52** 2995
[24] Savrasov S Y 1996 *Phys. Rev.* B **54** 16470
[25] Vosko S H, Wilk L and Nusair M 1980 *Can. J. Phys.* **58** 1200
[26] Bambynek W, Crasemann B, Fink R W, Freund H-U, Mark H, Swift C D, Price R E and Rao P V 1972 *Rev. Mod. Phys.* **44** 716
[27] Keski-Rahkonen O and Krause M O 1974 *At. Data Nucl. Data Tables* **14** 139
[28] Maris G, Ren Y, Volotchaev V, Zobel C, Lorenz T and Palstra T T M 2003 *Phys. Rev.* B **67** 224423
[29] Yamaguchi S, Okimoto Y and Tokura Y 1996 *Phys. Rev.* B **54** R11022
[30] Rehr J J and Albers R C 2000 *Rev. Mod. Phys.* **72** 621